JOURNAL OF GEOPHYSICAL RESEARCH, VOL. 113, F02S90, doi:10.1029/2006JF000585, 2008

Geophysical mapping of ground ice using a combination of capacitive coupled resistivity and ground-penetrating radar, Northwest Territories, Canada

Gregory P. De Pascale,[1,2] Wayne H. Pollard,[1] and Kevin K. Williams[3,4]

Received 14 June 2006; revised 26 July 2007; accepted 28 November 2007; published 10 April 2008.

[1] The nature and distribution of ground ice are two of the most unpredictable geological variables in near-surface deposits characterized by continuous permafrost. Subsurface information about ground ice distribution and structure can be obtained either by invasive and environmentally destructive techniques like drilling and excavation or by noninvasive low-impact geophysical methods. In this study, coordinated measurements by two complementary geophysical tools, capacitive-coupled resistivity (CCR) and ground-penetrating radar (GPR) were used to map ground ice in a variety of locations in the Mackenzie Delta region of the western Canadian Arctic. Both CCR and GPR systems are highly portable (especially on snow covered surfaces) and very effective in collecting data under winter conditions when cold ground temperatures ensure that nearly all liquid water is frozen and signal penetration is enhanced. CCR and GPR readily detect stratigraphic differences including the contacts between massive ice deposits and enclosing sediments. GPR is widely used in permafrost research, but CCR has been used in only a few studies. This is the first study to combine results from both systems by collecting complementary data sets along coincident transects. We demonstrate that when combined, these data increase the quality and interpretation of subsurface information beyond what could be determined by either of the instruments alone. The complementary nature of these two geophysical tools facilitated the detection and mapping of massive ground ice, ice-rich sediments, ice wedges, thermokarst, and basic stratigraphic relationships. This study breaks new ground by documenting the benefits of using these techniques together in permafrost investigations.

Citation: De Pascale, G. P., W. H. Pollard, and K. K. Williams (2008), Geophysical mapping of ground ice using a combination of capacitive coupled resistivity and ground-penetrating radar, Northwest Territories, Canada, *J. Geophys. Res.*, *113*, F02S90, doi:10.1029/2006JF000585.

1. Introduction

[2] Permafrost is a geological condition defined exclusively in terms of ground temperature and refers specifically to soil or rock that remains below 0°C continuously for a period of 2 years or longer. It forms when the ground cools sufficiently in winter to produce a layer that remains cryotic, or below 0°C, through the following summer [*Permafrost Subcommittee*, 1988]. Ground ice is a common constituent of permafrost but is not a prerequisite for its occurrence. The nature and distribution of ground ice is one of the most unpredictable and problematic geological variables in near-surface deposits characterized by continuous permafrost [*Pollard and French*, 1980]. The formation of ground ice is a complex process in which temperature, soil grain size and water content, chemistry, and transfer processes combine to determine the type and rate of ice formation. The many factors that contribute to the formation of ground ice influence the spatial pattern of ice occurrence and result in volumetric ice contents ranging from close to zero to nearly one hundred percent over relatively short distances and with little or no indication on the ground surface. The spatial variability and unpredictability of ground ice, together with the lack of surface expression of its occurrence, are one of the greatest problems facing northern development [*Pollard and French*, 1980]. Because of the uneven and unpredictable nature of ground ice distribution, there is a need for quick, noninvasive alternatives to drilling as a means of obtaining subsurface information. In this study, two geophysical tools, capacitive-coupled resistivity (CCR) and ground-penetrating radar (GPR), were used to map ground ice occurrence on and around Richards Island in the western Canadian Arctic. The primary goals of this paper are (1) to characterize ground ice conditions for a series of location on Richard Islands in the Mackenzie Delta and (2)

[1]Department of Geography, McGill University, Montreal, Quebec, Canada.
[2]Now at William Lettis and Associates, Inc., Earth Science Consultants, Walnut Creek, California, USA.
[3]Center for Earth and Planetary Studies, National Air and Space Museum, Washington, D. C., USA.
[4]Now at Department of Earth Sciences and Science Education, Buffalo State College, Buffalo, New York, USA.

0148-0227/08/2006JF000585$09.00

to demonstrate the complementary nature of GPR and CCR data in the analysis of ice-rich permafrost.

2. Background

[3] The term "ground ice" refers to "all types of ice formed in freezing and frozen ground" [*Permafrost Subcommittee*, 1988, p. 46]. A widely used ground ice classification developed by *Mackay* [1972] identifies three primary sources of water leading to ten genetically distinct types of ground ice. In this classification, ground ice occurrence ranges from disseminated ice crystals in a soil matrix (pore ice) to discrete V-shaped linear networks of vertically foliated ice (wedge ice) to thick (10–20 m), horizontally continuous layered bodies of nearly pure segregated ice that often extends for several square kilometers. Although frequently described in the Russian literature, "buried (surface) ice" was conspicuously absent from Mackay's classification. However, buried ice along with intrasedimental ice (i.e., combined segregated and intrusive ice) was included by *Mackay and Dallimore* [1992] as the main types of massive ice. Massive ground ice is defined as ice greater than 1 m thick with a gravimetric water content exceeding 250% [*Permafrost Subcommittee*, 1988]. This form of ground ice is sometimes encountered in coarse-grained fluvial-glacial sediments found in the western Canadian Arctic [*Gowan and Dallimore*, 1992; *De Pascale*, 2005]. Pore ice, wedge ice, intrasedimental ice, and buried ice are most significant in terms of ice volume and frequency of occurrence.

[4] The analysis of ground ice occurrence is significant for two reasons: first, from the environmental perspective because knowledge about its origin provides insight into poorly understood aspects of permafrost and ground ice geomorphology, landscape evolution and paleoclimate. And second, from the engineering and management perspectives because knowledge of ground ice distribution is necessary to avoid human induced thaw subsidence (thermokarst) of ice-rich ground. The latter is an important aspect of this study because two of our field sites are likely to be exploited as sources of sand and gravel for the Mackenzie Valley Gas Project.

[5] Thermokarst is a potentially important erosional process unique to areas underlain by ice-rich permafrost. The significance of thermokarst is often expressed in terms of its impact on human activities (e.g., construction of pipelines and highways) or as a response to global warming. However, it should be remembered that thermokarst is a naturally occurring process that plays a key role in polar landscape development. The nature and magnitude of thermokarst is directly related to two variables: (1) the thermal stability of the upper part of permafrost, including the depth of the active layer, and (2) ground ice contents. Two types of thermokarst are described in the literature: (1) thermokarst subsidence and (2) thermal erosion. Thermokarst subsidence is primarily vertical in direction and involves down wearing, whereas thermal erosion involves lateral planation and is a back-wearing process [*Pollard*, 2005].

3. Study Area

[6] Our field program focused on kame and fluvial-glacial deposits in the Richards Island area of the western Canadian Arctic. Richards Island forms part of the Pleistocene Mackenzie Delta (Figure 1) and consists of undulating tundra terrain, usually less than 50 m above sea level (masl). It is situated along the western Canadian Arctic coast within continuous permafrost whose thickness often exceeds 400 m [*Mackay*, 1963]. Mean annual air temperature is approximately -11°C (Environment Canadian, Climate Normals 1971–2000, http://www.climate.weatheroffice.ec.gc.ca/climate_normals/, last accessed 2 November 2004) while ground temperatures generally range from −7 to −10°C [*Mackay*, 1998]. Ice wedge polygons are ubiquitous, and the numerous pingos, tundra ponds and retrogressive thaw slumps are a constant reminder of the dynamic role permafrost plays in this part of the Mackenzie Delta [*Mackay*, 1979, 1998]. The Mackenzie Delta region is widely recognized as one of the most ice-rich permafrost regions in the Arctic [*Mackay*, 1963, 1972], and the volume of ground ice present in the upper 10 m of Richards Island has been estimated to be 10.3 km^3 [*Pollard and French*, 1980]. In some cases the stratigraphic setting and origin of the ground ice reflects a complex history of permafrost aggradation and glacial activity [*Murton et al.*, 2004, 2005].

[7] The climatological records for Tuktoyaktuk show no appreciable change in trend in summer climate between 1960 and 1999; however, winter and daily mean temperatures showed an increase between 1960 and 1980 [*Mackay*, 1999]. The ice-rich nature of permafrost in the Mackenzie Delta together with anticipated climate warming is a major concern for this region. Furthermore, proposed pipeline development on Richards Island associated with the Mackenzie Valley Gas Project makes the need for information about ground ice distribution a high priority.

[8] Fieldwork focused on fluvial glacial deposits identified as potential granular resource sites or locations where ice-rich coarse-grained deposits had been mapped [*EBA Engineering Consultants Ltd.* (*EBA*), 1987; *Rampton*, 1988]. Because one of our main research goals was to assess the nature and distribution of ground ice in coarse-grained deposits in the Mackenzie Delta, we selected two sites (DIAND sites 208 and 303) identified as potential granular resources in a report prepared for the Department of Indian and Northern Affairs Canada. Each of these sites is clearly located in the report [*EBA*, 1987] and described in terms of their granular resource potential, including varying amounts of information on structure, stratigraphy, and ice content. These data were essential as a calibration reference for our geophysical data. As an independent test of our methodology, we identified an additional site mapped as ice-rich fluvial glacial material based on surficial geological mapping by *Rampton* [1972, 1979, 1988]. This outwash site corresponded with an area where active hydrocarbon exploration was underway and provided access to a recently excavated sump. Most of the sites were accessed using the network of ice roads along the Mackenzie river and in one case a winter road traversing Richards Island was used to access an active sump site (Figure 1) in support of an ENCANA drilling operation. Ground ice is present at all three sites, and in each case there are distinctive geomorphic features related to massive ice such as stabilized thermokarst and wedge ices.

4. Methods and Data Acquisition

[9] Ground resistivity and radar techniques give valuable information about subsurface conditions based on

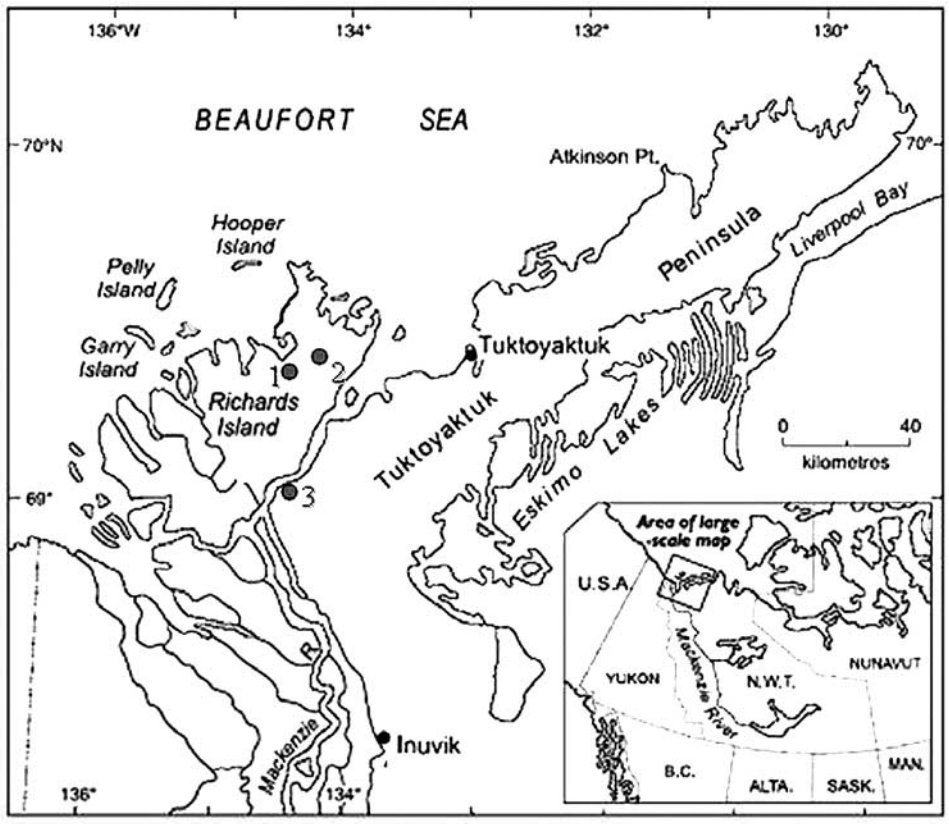

Figure 1. Study site locations in the Mackenzie Delta Region of the Canadian Arctic; 1, Site 208; 2, Outwash site; 3, Site 303.

different electromagnetic properties of sediments. Electrical resistivity determines the subsurface resistivity distribution from induced current measurements made at the ground surface. From these measurements, the specific resistivity of the subsurface can be estimated. Ground resistivity is related to various geological parameters such as mineralization and fluid content, temperature, porosity, and degree of water saturation in rocks or unconsolidated sediments. The resistivity of a material can be calculated using Ohm's law:

$$R = V/I(\text{resistance} = \text{voltage}/\text{current}) \quad (1)$$

For geoelectrical measurements of ground resistivity Ohm's law is used in its differential vector form:

$$\rho = E/J \quad (2)$$

where ρ is resistivity, E is electric field, and J is current density. By measuring an electric field at a known current, it is possible to calculate the resistance of the total volume of material between the transmitter and receiver to the depth of detection limit of the transmitter signal [*Loke and Barker*, 1996].

[10] Resistivity techniques work well in regions of permafrost because of the marked increase in electrical resistivity of water that occurs at the freezing point [*Hoekstra et al.*, 1975; *Wolfe et al.*, 1996; *Calvert et al.*, 2001; *Calvert*, 2002; *Hauck*, 2002; *Hauck et al.*, 2003]. In permafrost regions resistivity will vary directly as a function of the ice content and type; for example, sediments with low ice contents are generally conductive and typically have low resistivity values. Sediments with high ice contents will generally have resistivities higher than sediments without ground ice but lower than sediments containing a massive ice body. In areas of weathered bedrock, the mineralogy of the rocks will strongly influence the resistivity values; however, bedrock is rarely encountered in this area of the Arctic.

[11] There are two types of resistivity surveys commonly used in permafrost environments: (1) direct current (DC), which uses galvanic coupling, and (2) capacitive-coupled resistivity (CCR). DC resistivity involves the placement of electrodes in the ground in a specific grid and then measuring the electrical potential between two electrodes while a current is applied to the ground via two other electrodes [*Hauck*, 2002]. Dry or frozen ground is difficult to measure with DC methods because high surface resistivity values create problems with grounding of the applied current [*Baines et al.*, 2002]. However, several recent studies [*Kneisel et al.*, 2000; *Ishikawa et al.*, 2001; *Marescot et al.*, 2003; *Hauck and Kneisel*, 2006] have shown that it is

Table 1. Typical Values for Dielectric Constant and Velocity for Common Geological Materials at 100 MHz[a]

Material	Dielectric Constant	Velocity (m/ns)
Dry sand	3–5	0.15
Ice	3–4	0.16
Frozen sediment	6	0.12
Saturated sand	20–30	0.06
Fresh water	80	0.033
Seawater	80	0.01

[a]See, e.g., *Davis and Annan* [1989] and *Moorman et al.* [2003].

possible to conduct effective DC surveys in mountain permafrost environments. DC methods can also be very time consuming in both preparation and survey time.

[12] Capacitive-coupled resistivity (CCR) surveys are a recent advancement in resistivity mapping technique. For a detailed review of the theory behind capacitive-coupled resistivity, see *Timofeev et al.* [1994]. As with DC resistivity, CCR uses two dipoles. In principal, current is applied to the ground by a transmitter via capacitive-coupling and the resulting potential is measured at the receiver dipole. The system is not dependent on surface contact and can be towed along the surface while collecting data, thus permitting faster data collection over large study regions (Figure 3). Two previous studies using CCR techniques in permafrost were not able to distinguish between massive ice and glaciofluvial sediment with ice contents >30% [*Wolfe et al.*, 1996], but *Calvert* [2002] noted that two-dimensional resistivity measurements were acquired relatively quickly in areas of ground ice. In another recent study, different resistivity techniques are compared in an area of mountain permafrost in the Swiss Alps [*Hauck and Kneisel*, 2006]. However, in this environment permafrost conditions are very different from the Mackenzie Delta region, for example midlatitude alpine permafrost is much warmer, wetter (higher liquid water content), contains little ground ice (extensive massive ice is largely absent) and bedrock plays an important control on landscape development. These are the only published studies to date involving CCR investigations in permafrost. *Wolfe et al.* [1996] and *Calvert* [2002] are both general and provide few details about data acquisition, processing, and interpretation while the latter focus on a different type of permafrost.

[13] Ground-penetrating radar (GPR) is another geophysical tool that has been used increasingly over the last 30 years for a wide range of subsurface mapping applications. By transmitting an electromagnetic pulse into the ground and recording the traveltime of reflections caused by contrasts in dielectric properties at stratigraphic boundaries or by discrete objects, GPR measurements are used to characterize the structure and stratigraphy of near-surface geology. GPR data are typically collected over a frequency range of ~10 to 1500 MHz, depending on the objectives of the study. Lower frequencies (longer wavelengths) will generally penetrate more deeply than higher frequencies, but higher frequency measurements have better vertical resolution for detecting closely spaced interfaces.

[14] Because of the low dielectric constant of ice compared to solid rock and sediments containing liquid water (Table 1), GPR has proven to be an excellent tool for studying glacial and permafrost regions. Previous studies have used GPR to study permafrost [*Doolittle et al.*, 1990; *Hinkel et al.*, 2001; *Moorman*, 1994, 1995; *Arcone et al.*, 1998; *Moorman et al.*, 2003], massive ground ice [*Dallimore and Davis*, 1987; *Dallimore et al.*, 1992; *Robinson*, 1994; *Robinson et al.*, 1992; *Wolfe et al.*, 1997], and glaciers [*Arcone et al.*, 1995; *Fountain and Jacobel*, 1997; *Murray et al.*, 1997; *Moorman and Michel*, 2000]. These studies have shown that GPR data reliably indicate contacts between ice and frozen sediments, ice and solid rock, and frozen and thawed regions. The large contrast in dielectric properties between ice and water also make GPR useful for studying seasonal changes in permafrost environments.

[15] In this study geophysical surveys were conducted in March 2004 with air temperatures between −15°C and −40°C, and the ground surface was covered by wind-crusted snow. Ground resistivity was measured using a Geometrics OhmMapper TR1 system, with operating frequencies in the range of 8 to 32 kHz using a dipole-dipole transmitter and receiver. Current is run along the transmitter's dipole cables with the dipoles acting as one plate of a capacitor and the ground as the other. The resulting voltage, measured at the receiver dipole, is proportional to the ground resistivity between the two dipoles and the initial current emitted from the transmitter. The OhmMapper system records transmitter current, resulting voltage, and geometry, with results displayed as apparent resistivity versus geometry. The apparent resistivities are calculated from the measured resistances using the geometric factor, which corresponds to the distance between the transmitter and receiver. Changing this separation changes the penetration depth, which is approximately 30% of the separation distance between the transmitter and the receiver using a TR1 system. Multiple passes are made along each survey line to gather data over a range of n spacings, which is the ratio of the distance between the transmitter and receiver and the dipole spacing, permitting resisitivity measurements of the materials at several depths. By increasing the distance between the transmitter and receiver, a larger survey line is created, giving a greater depth of investigation. Although not used in this study, an alternative setup employs a series of receivers in a train with different n spacings to collect sufficient data in one pass. In this study the initial n spacing was used for two passes at each site in order to ensure data reliability and measurement consistency.

[16] The GPR system used was a Geophysical Survey Systems, Inc. (GSSI) SIR-3000 GPR controller with antennas operating at 200 MHz (λ = 1.5 m) and 400 MHz (λ = 75 cm). At some sites we also collected data with a 900 MHz antenna (λ = 33 cm) to record finer near-surface structures. The SIR-3000 controller is a very portable system worn in a harness as the antenna is pulled across the surface. The controller triggers pulses of energy that are transmitted into the surface by the antenna which acts as a band-pass filter emitting sine waves with the center frequency determined by the antenna. Since penetration depth of a GPR signal depends on the antenna frequency and the electromagnetic properties of the subsurface materials, the frozen ice-rich nature of our sites were favorable for penetration depths on the order of ~10 m at the frequencies used. A Trimble 5700 differential global positioning

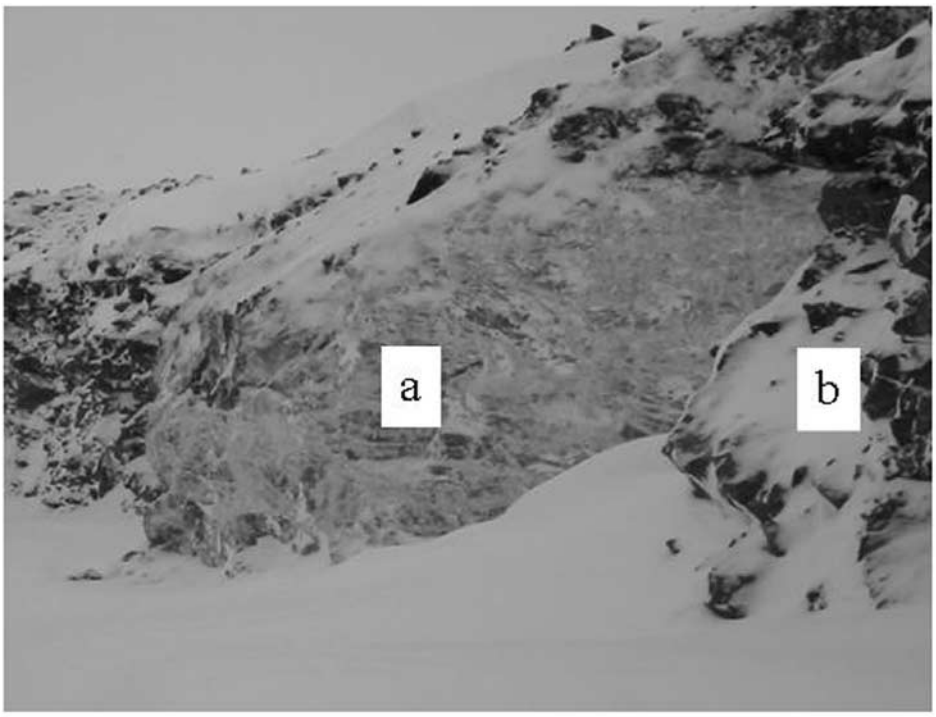

Figure 2. The sump exposure found adjacent to the survey transect at the outwash site. Note the massive ice body (label a) enclosed in frozen sand (label b). The exposed ice body is ~4 m thick.

system (DGPS) was used for topographic corrections in this study.

5. Data Processing

[17] The CCR data were reduced using the DataMap 2000 software [*Geometrics*, 2001], while inversions were completed using the two-dimensional inversion software RES2DINV [*Loke and Barke*, 1996; *Loke*, 1999]. These CCR data were transferred to RES2DINV where filtering techniques such as despiking were employed to remove outliers and smooth the data sets with a three-point running average. Data were plotted in a pseudosection, where the depth scale is calculated as a function of the separation between the dipoles. A pseudosection is a geometrical view of the measured apparent resistivity data set, whereas the inversion model shows the true resistivity for each model block, which is calculated independent of the resistivities of the surrounding model blocks. An inversion of the resistivity data is useful in creating a subsurface model of the stratigraphy for each site including ground ice features like bodies of massive ground ice and ice wedges. Interpretations of the CCR models were constrained by other subsurface information available at each of the sites, including bore hole data and test pits collected during initial granular resource assessments.

[18] GPR data were processed using the RADAN software package by GSSI.Processing involves time–zero surface correction and horizontal filtering of the direct coupling wave. This processing is standard for GPR data and removes system noise that could mask real data. Because of the frozen nature of the field sites, penetration depth estimates assumed a dielectric constant of 6 (v = 0.12 m/ns) for frozen sediments and a dielectric constant of 3 (v = 0.16 m/ns) for ice as shown in Table 1. These assumptions were reinforced by previously collected borehole data [*EBA*, 1987] and an exposure of frozen sand and massive ground ice at one site. Field measurements of topography can also be used to correct GPR transects from areas with elevation changes, providing a more realistic presentation of subsurface structure and stratigraphy.

[19] The comparing of two different geophysical data sets for the same site is not a straightforward process, even when the data are collected at the same time. Because of the differences in properties between GPR and CCR data and the way the respective software packages process these data, several modifications of the processed data were made to produce an integrated output. Problems with scaling the two data types were encountered as each of the processing software packages produce outputs that are scaled differently. Aligning the CCR and GPR data outputs was done graphically by aligning both horizontal and vertical scales for each transect. The survey sites are discussed in detail in the following section.

6. Results

6.1. Site 1: Outwash Site

[20] Site 1 is an area of glacial fluvial sediment that had been excavated for use as a drill fluid sump. The sump is located at 69°25′30″N, 134°8′77″W in the center of a mapped glacial outwash channel [*Rampton*, 1988]. It is approximately 100 m long by 30 m wide and 10–15 m deep. The sump provided access to a massive ice section exposed in the southern wall of the excavation (Figure 2). A stratigraphic section, including the massive ice body, was

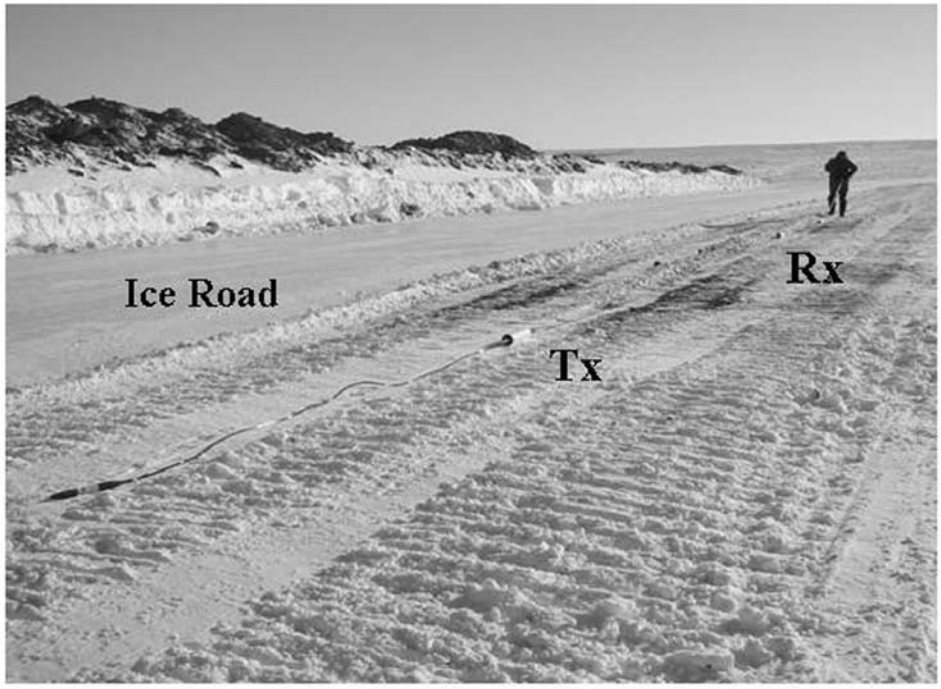

Figure 3. CCR data being collected along survey line at the outwash site. The left side is west, and the right side is east. The transmitter (Tx) and receiver (Rx) are shown. The sump in Figure 2 is located 4 m to the left (north) of ice road.

mapped and sampled at 1-m intervals for geochemical and petrographic analysis [*De Pascale*, 2005]. The general stratigraphy of this site included a thick layer of nearly pure ice and icy sand conformably overlain by 2–3 m of horizontally bedded ice-bonded fine sand. The massive ice contained vertically oriented and elongated gas inclusions perpendicular to the surface, possibly suggesting an intrasedimental origin, although the irregular blocky structure suggests a buried ice origin.

[21] The geophysical surveys were conducted parallel to the exposure (Figure 3) so that the data could be compared directly with known stratigraphic and cryostratigraphic information. The CCR survey used n spacings of: 0.25, 0.5, 0.75, 1.0, 1.5, 2.5, 3.0, 3.5, 4.0, 5.0, 6.0, 7.0, and 7.5. Measured resistivity values ranged from 10,000 to 25,000 Ohm m at depths corresponding with the massive ice body, while values between 6,000 and 10,000 Ohm m were measured at depths characterized by frozen sand. The upper contact of the massive ice was planar to wavy and underlying the highly resistive region (~18,000 to ~40,000) below the surface (~1–2 m) of the profile, corresponding to ice on the winter road and pore and segregated ice in the active layer (Figure 4a). Contrasting resistivity values in the CCR data correspond with the locations of the; frozen active layer, massive ice body, and frozen fluvial-glacial sand at the site. The geometries of each of these materials in the CCR models closely resemble (Figure 4a) the structures found in the nearby exposure (Figure 2). The top of the massive ice was detected at a depth of ~3 m in the CCR data.

[22] GPR data were collected using 400 and 200 MHz antennas along a 90-m transect (Figures 5a and 5b). The data show strong reflectors at two levels, with the upper reflections being mainly horizontal and extending to a depth of ~25 ns and the lower interface appearing at ~50 ns and exhibiting more variations in topography. Stratigraphic information from the sump wall was used to help guide the interpretation. The region between the two areas of high reflection contains semihorizontal structures. Figure 5c shows an interpretation of the 200 MHz data where strong reflections have been traced and material interpretations have been labeled. Estimated depths were calculated using a velocity of 0.14 m/ns assuming a combination of frozen sediments and areas of massive ice. Using these depths, the upper reflections extend to ~1.75 m and the tops of the lower reflections are at ~3.5 m. As noted above, the upper reflections likely represent material associated with the ice road and the active layer. The semihorizontal structures below the active layer may represent layering of ice in frozen sediments. The lower reflections are interpreted as the tops of 2–3 separate massive ice bodies, possibly buried glacier ice, Pleistocene ground ice, or Pleistocene ice wedges [*Murton and French*, 1994]. Although similarities in dielectric properties between ice, sand, and frozen sand present the possibility for ambiguities in data interpretation, background knowledge about the surficial geology and permafrost history of this site, as well as the stratigraphic exposure in an adjacent sump, permit confident interpretation of the GPR data.

[23] Both geophysical methods yielded stratigraphic information marked by ranges in electrical properties known to correspond with permafrost and ground ice that provide the basis for our interpretation. CCR data mapped the distribution and geometry of ice, and GPR data showed stratigraphy associated with the pattern of ground ice distribution. Figure 6a shows the CCR transect combined

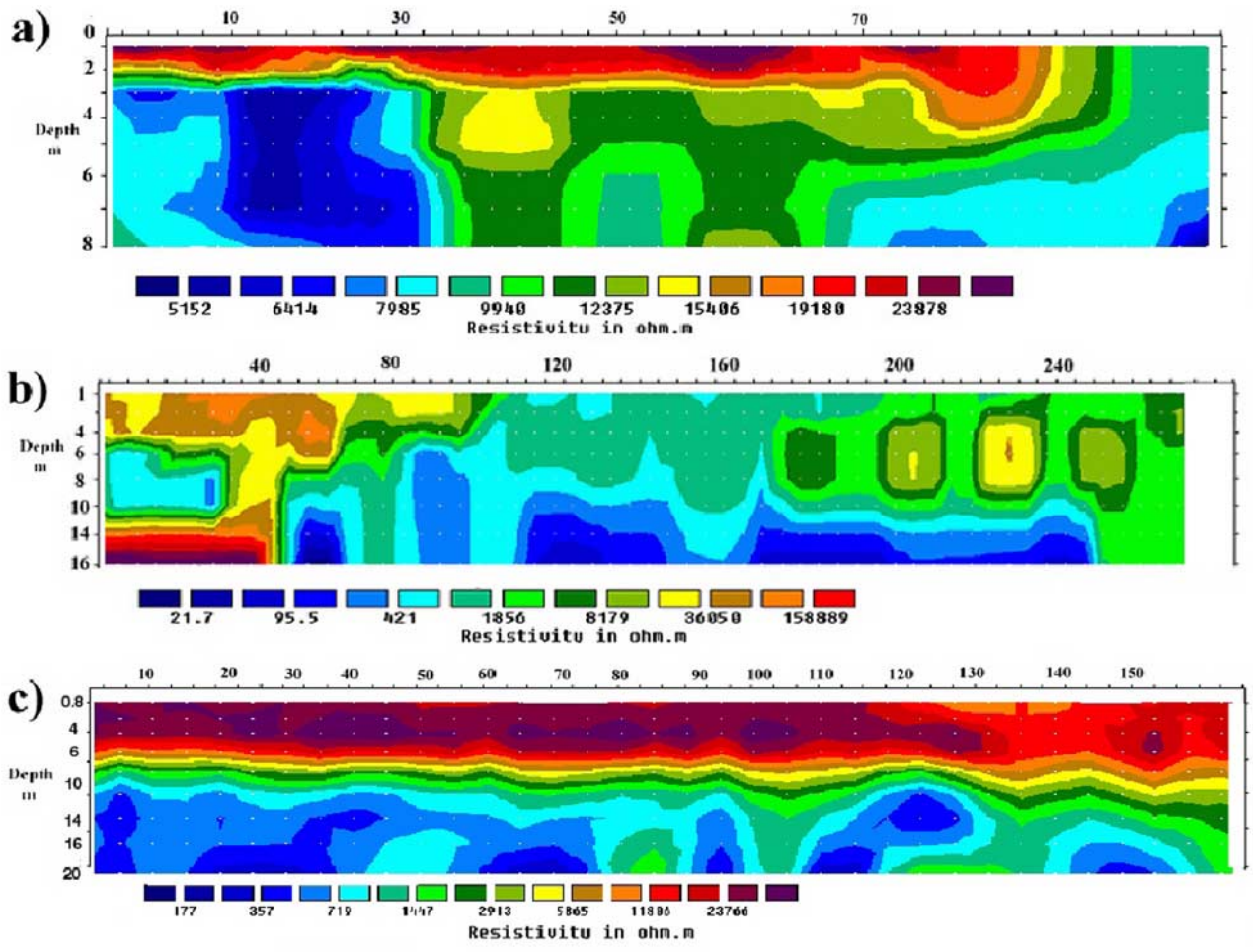

Figure 4. Subsurface resistivity inversion models for the (a) outwash site with RMS = 16% (with left being west and right east), (b) Site 208 with RMS = 19% (with left being west and right east), and (c) Site 303 with RMS = 22% (with left being west and right east). Range of resistivity values are shown for each site.

with the GPR interpretation (Figures 5b and 5c). To obtain close correspondence, it was necessary to adjust the GPR output. Figure 6b presents a revised interpretation of the integrated data where two "possible" ice bodies in the GPR interpretation have been removed based on the CCR. Ghost reflections are not uncommon in GPR data. By combining these two data sets, the subsurface ice distribution and structure can be interpreted beyond what was possible with either data set alone.

[24] Both systems detected strong electromagnetic interfaces interpreted as the base of the active layer and a contact between massive sand and massive ground ice, and there is a high correlation in the stratigraphic positions and depths of these contacts in the CCR and GPR transects. Stratigraphic and cryostratigraphic mapping of the nearby sump wall provided validation of the geophysical data; however, as typical in many sections (both natural and excavated) the lower ice contact was not visible.

6.2. Site 2: Granular Resource Site 208

[25] Another Richards Island site studied with both CCR and GPR and located at 69°24′28″N, 134°18′45″W at an elevation of 58 masl (Figure 1). This location has been mapped as a glaciofluvial kame deposit [*EBA*, 1987] with low ice contents and is also probably related to the Toker Point Stade [*Rampton*, 1972, 1988]. Subsurface information about this site is sparse, consisting of only one shallow test pit for the entire feature. On the basis of that one test pit, the subsurface material was described as frozen sand with a 30% ice content.

[26] The geophysical transect ran 280 m from south to north along the long axis of the kame ridge from the top of a knoll through a small depression to the summit of another small knoll (Figure 7). On the basis of the smooth nature of slopes and the gradual change in relief, the topographic variation was initially interpreted to be a function of depositional history. Resistivity data were collected using dipole n spacings of 0.5, 1.5, and 3.0 and the survey site was covered by approximately 0 to 1 m of hard-packed snow. The CCR survey data (Figure 4b) indicate a high resistivity layer (~5 m thick) beneath both elevated surfaces but pinching out (lower resistivity values) beneath the depression. Data interpretation suggests the presence of either massive ice or ice-rich materials beneath the elevated

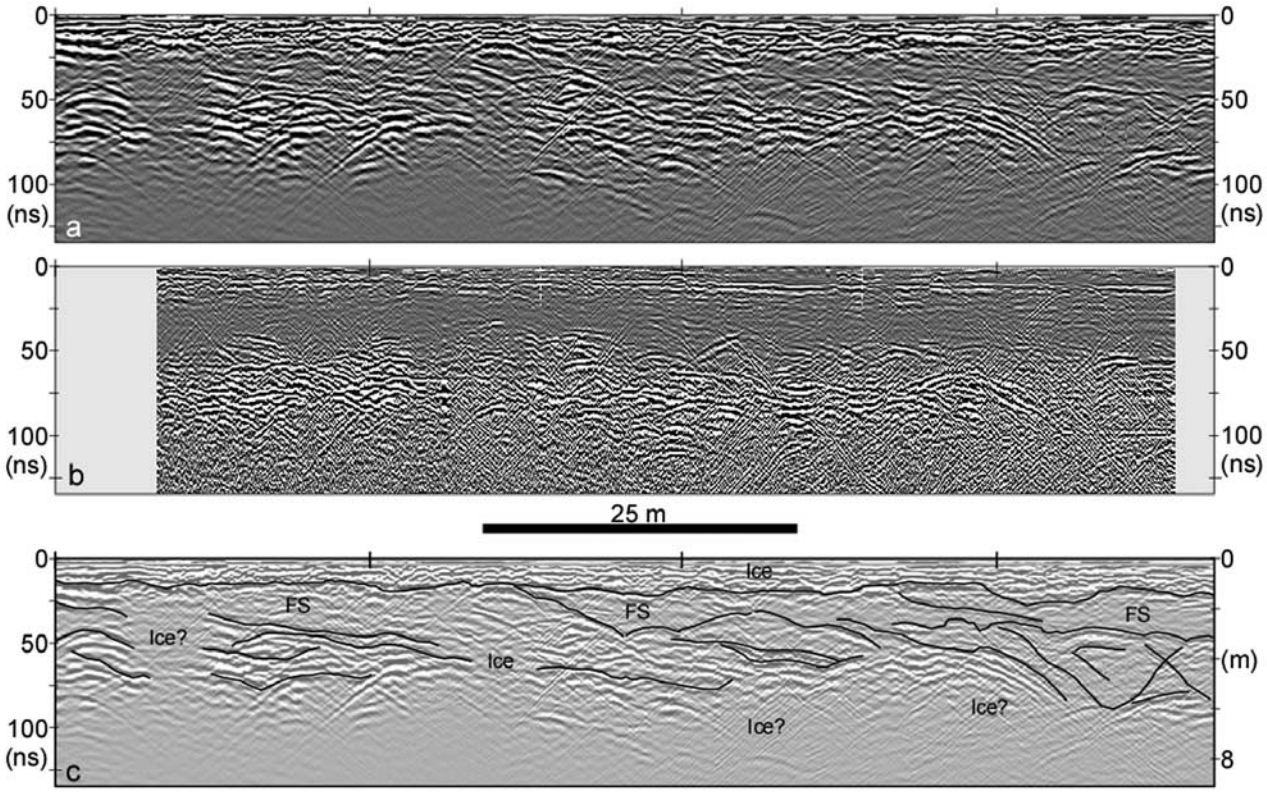

Figure 5. GPR data collected at (a) 200 MHz and (b) 400 MHz collected at the outwash site. The left side is west and the right is east. The 400 MHz transect was slightly shorter than the 200 MHz transect. (c) Interpretation delineates major contacts, and regions of different materials are labeled as frozen sediments (FS) and massive ice. Several possible bodies are also labeled, and comparison with CCR data (Figure 6) will help refine initial interpretations. Depth estimate is based on a signal velocity of 0.14 m/ns.

portions of the kame ridge and little or no ground ice beneath the depression (Figure 4b). The very high resistivities encountered in the first 40 m of this transect are likely an artifact of the inversion process. These ice-rich materials lie between 3 and 8 m below the surface in the northern part of the transect.

[27] GPR data were collected at 200 and 400 MHz along a 300 m transect (Figure 8a). Topographic data were also collected and are used to compare subsurface reflections to topography in order to aid in interpretation (Figures 8b and 8c). Reflections sloping toward the center of the transect correspond to the edges of the surface depression and likely denote stratigraphy consistent with thaw subsidence (thermokarst). Strong reflectors are present toward the two ends of the transect, situated under topographic high points. Reflections in the left (south) side of the transect occur in a block ~50 m wide, whereas large reflectors along the northern part of the transect occur in three or four 10-m-wide blocks. Figure 8b shows an interpretation of the data where depth is estimated using a velocity of 0.12 m/ns for frozen sediments. Ice bodies are located based on the assumption that areas of muted or interrupted reflections represent subsurface massive ice bodies [*Moorman et al.*, 2003]. An area of herringbone reflections ~175 m from the left end of the transect is interpreted as small ice lenses [*Moorman et al.*, 2003]. There were no structures under the depression that would have suggested massive ice bodies there.

[28] As with the outwash site, CCR and GPR data are combined to take advantage of the benefits of coincident geophysical transects (Figure 6c). The most significant result of combining the two data sets for this location is the adjustment of locations for some of the ice bodies in the northern part of the transect. The fusion of CCR and GPR results shows that the strong reflections only sometimes correspond to high ice concentrations and sometimes do not. For Site 208, identification of ice concentrations with CCR data has helped distinguish more GPR representations of ice than previously reported in the literature [*Moorman et al.*, 2003]. In addition, the expanded interpretation from the combined data sets supports the theory that the depression resulted from thaw subsidence. Without the GPR data at this site, the CCR data suggests lack of massive ice due to depositional variations, not due to postdepositional thermokarst. Thus, the combination of these techniques yields information concerning thermokarst that would not be possible with one instrument alone.

[29] It should be noted that the test pit information [*EBA*, 1987] is highly misleading if taken to represent the entire deposit. Data from this study indicate ice contents well in excess of the ~30% suggested in the EBA consultants report, strongly reinforcing the potential limitation of their approach.

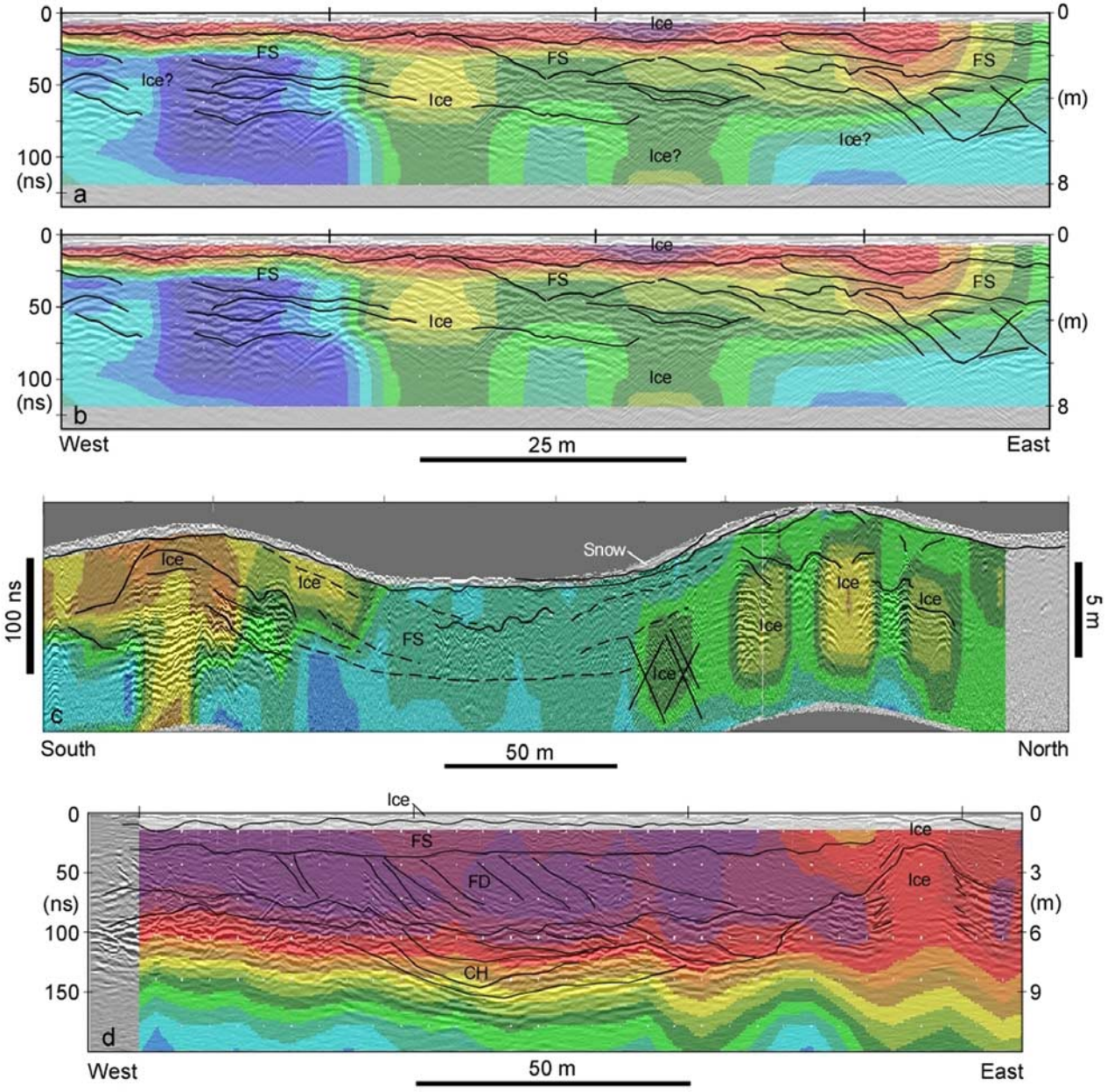

Figure 6. Combined CCR and GPR data for the three field sites. (a) Outwash site CCR combined with interpreted GPR data (Figure 5c). Note that two of the ''ice''? locations correspond to areas of low ice concentration based on CCR data. (b) Combined data for the outwash site where GPR interpretations have been slightly modified based on additional information from the CCR ice distributions. (c) Combined data sets for Site 208. CCR data have been fit to the topographic data, and the GPR interpretations in Figure 8c have been modified following fusion with the CCR data. Vertical scale bars apply only to the subsurface. Northern hill is ~6.7 m above the depression. (d) CCR and GPR data for Site 303. Fewer adjustments were necessary in this case, but combination of the two data sets reveals an interesting relationship between stratigraphy and ice content. See text for discussions of interpretations from the combined data sets. Compass directions are given for each transect.

[30] The elevated portions of our transect at this site appear to owe much of their relief to the presence of ground ice, whereas the depression is interpreted to be the result of thaw subsidence. This interpretation is supported by reflections in the GPR data that dip toward the depression. In addition, the difference in surface elevation correlates directly with the thickness of the massive ice/ground ice layer in the geophysical data.

6.3. Site 3: Granular Resource Site 303

[31] Survey Site 303 is on the eastern side of the Mackenzie River's East Channel (69°03′22″N, 134°33′40″W),

Figure 7. Transect of the resistivity and GPR surveys at Site 208. The surveyor is facing north and standing in the center of what appears to be a thaw depression.

just south of Swimming Point on the southeast corner of Richards Island (Figure 1). It is mapped as a glaciofluvial sand deposit with varying ice contents ranging from no visible ice to 7 m of massive ice, based on twelve separate boreholes [*EBA*, 1987]. Compared to the other field sites, this site had the most available background information. We designed our survey to maximize the available data, so our transect was located close to borehole 303 A-1 [*EBA*, 1987]. This borehole log indicated a surface unit with 3.5 m of sand and gravel with ice contents <20% underlain by 6 m of silty massive ice, which was then underlain by silt. The site was characterized by a relatively flat to gently rolling terrace surrounded by several small lakes. The surface was covered with hard packed snow ranging from a few cm to 1 m in depth, and a series of ice wedge troughs intersected the transect (Figure 9). Resistivity data were collected using dipole n spacings of 0.25, 0.5, 0.75, 1.0, 1.5, 2.5, 3.0, and 3.5 over a 150 m transect (Figure 4c). The resistivity data clearly indicate the nature and size of the ice wedges between 0.5 m and 6 m below the surface. Areas beneath surface expressions of ice wedges correspond with

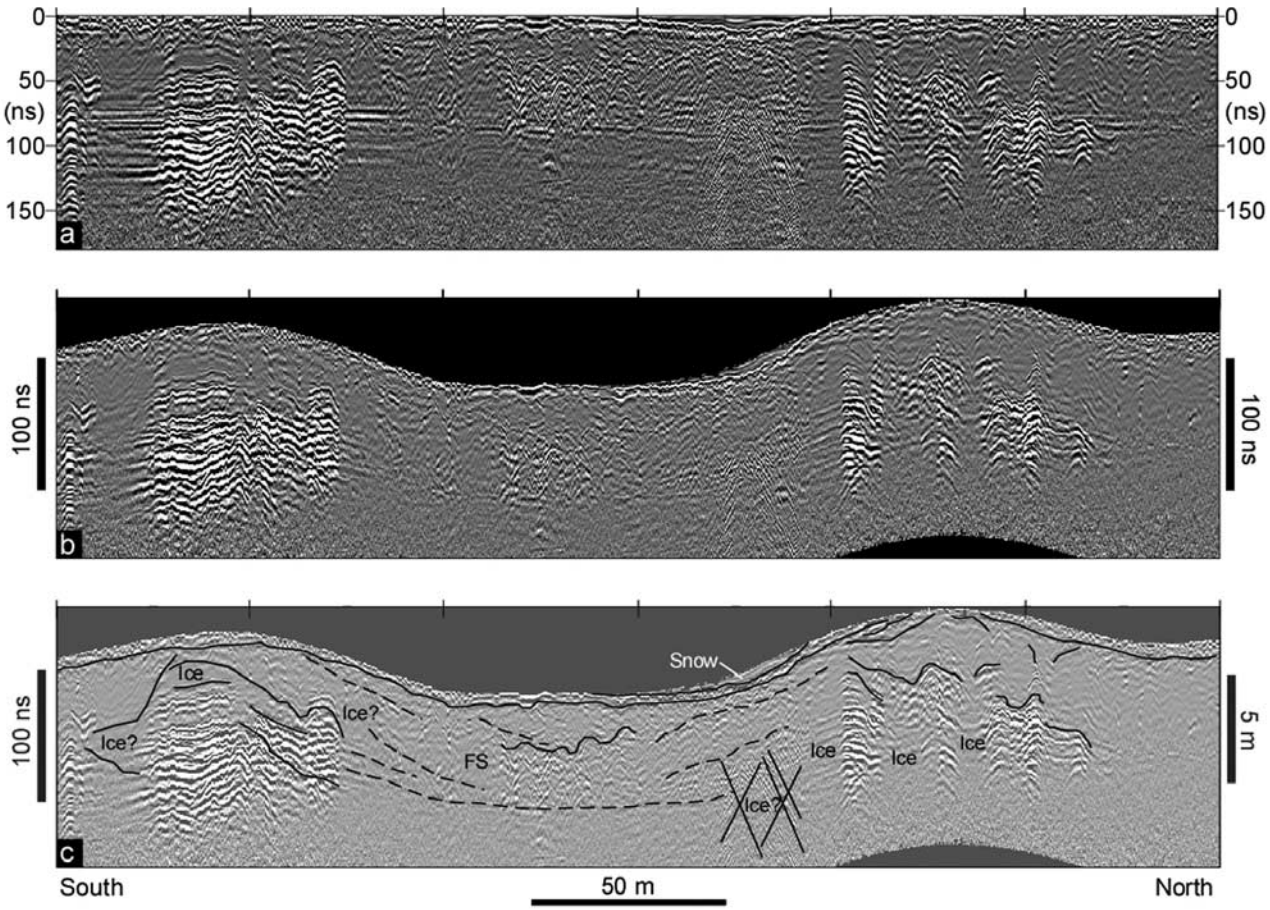

Figure 8. (a) The 200 MHz GPR transect from Site 208. 400 MHz data show similar subsurface information. (b) The 200 MHz data corrected for topography as measured with GPS. (c) Interpretation showing strong interfaces including stratigraphy dipping toward the center of the depression (dashed lines). The interpretation includes ice bodies in the southern and northern portions of the transect but only frozen sediments (FS) beneath the depression. Tick marks across the tops of the figures are spaced at 50-m intervals. Vertical scale bars apply only to the subsurface. Northern hill is ~6.7 m above the depression.

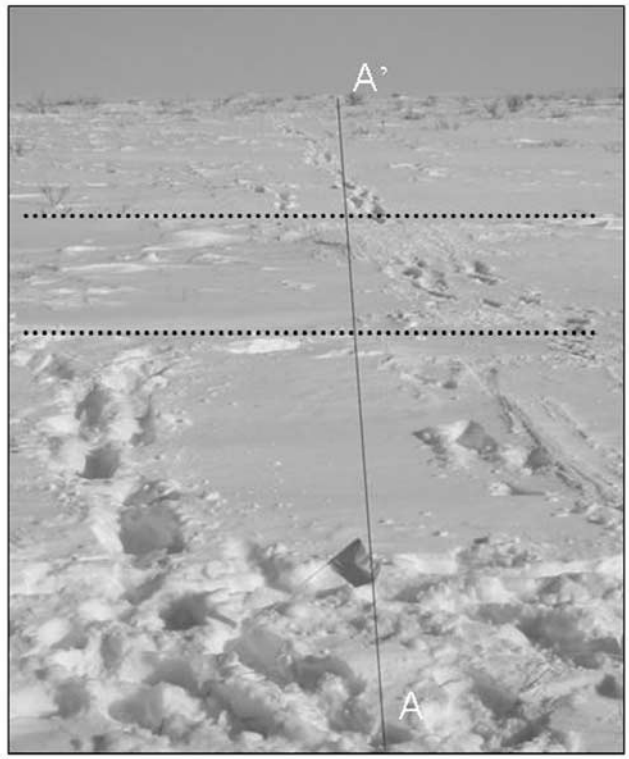

Figure 9. Location of survey at Site 303. Dotted parallel lines indicate locations of snow-filled ice wedge troughs encountered during the survey. The photo was taken toward the east.

the highest resistivities (15,000–30,000 Ohm m), which is expected for wedge ice. Zones of high resistivity adjacent to the ice wedges are interpreted as zones with higher ice contents or possibly relict ice wedges. There is a sharp planar boundary at ~9 m depth between the ice wedge features and the underlying deposits where the resistivity of the sediments is very low. These low resistivity values, between 380–3,000 Ohm m, suggest that the silt under the wedges and pore ice is very ice poor.

[32] CCR results are consistent with borehole data, which indicated massive ice bodies extending to 9 m below the surface [*EBA*, 1987]. However, borehole data showed low ice contents in the top ~3 m, but CCR data revealed high amounts of ice in the top 3 m. The RMS value for this site, as with the other sites in this study was likely influenced by the large variance in resistivity encountered in ice-rich permafrost. CCR data also reveal the presence of ice wedges as discrete bodies of highly resistive material but do not define the wedge ice geometry very accurately.

[33] As with the previous two sites, GPR data were collected at 400 and 200 MHz over a 170-m transect. In addition, data were collected at 900 MHz along a portion of the track in an attempt to map in more detail the structure of ice wedges that were located from their surface expression. The 400 and 200 MHz data reveal a wider range of structures below the surface than at the other two sites (Figure 10a), likely resulting from a more complex history in the near surface at this site. Assuming a velocity of 0.12 m/ns for frozen sediments, Figure 10b shows that strong reflections were detected to depths of at least 10 m. The top 1 m contains reflections that likely correspond to the active layer. Below that layer and extending to a depth of ~2 m are fairly horizontal layers. These layers are in contrast to deeper, tilted layers that are interpreted as foreset bedding due to deltaic processes [e.g., *Moorman et al.*, 2003]. These deposits occupy depths of ~2 to 6 m along much of the transect and also exhibit features below the surface depressions that indicate wedge ice. Below ~6 m depth, reflections again appear fairly horizontal except in areas of concave-up reflections suggestive of a channel that existed prior to deposition of the foreset bedding (Figure 10b). The eastern ~40 m of the transect does not exhibit the above structures. Instead, a dome-like reflection rises to ~1 m below the surface. Otherwise strong reflections become faint below the peak of this feature, suggesting the presence of a body of massive ice.

[34] The hatched box in Figure 10b shows the location of the 900 MHz data (Figure 10c). Those data reveal the top ~75 cm of the surface in the area where ice wedges were expected. The top of that profile shows the ground surface below varying thickness of snow, and the rest of the profile shows the active layer. At 900 MHz, at least three ice wedges are identified based on abrupt changes in topography of the ground surface or near-vertical disruptions in horizontal reflections.

[35] When combined with the resistivity data, the stratigraphy described above can be linked directly to the distribution of ice (Figure 6d). This comparison shows that very high ice concentrations are coincident with the upper horizontal layers (FS) and the foreset deposits (FD). The transition to very low ice contents occurs just below the reflections interpreted as a paleochannel. The area interpreted as a possible massive ice body has resistivity values lower than elsewhere in the transect but still consistent with ice. This could be due to an underestimation of the thickness of the high-resistive layer in the CCR model inversion, which has been found in other resistivity studies in permafrost [*Hauck*, 2002; *Hauck et al.*, 2003] Again, a combination of CCR and GPR data results in a more complete description of the subsurface than would have been possible with only one data set.

7. Discussion

[36] Geophysical techniques, like most forms of remote sensing, are highly subjective and vulnerable to interpreter error. This is particularly true for geologies affected by permafrost where the inclusion of ground ice, small amounts of liquid groundwater and cryogenic structures complicate interpretation. With the ever expanding use of geophysical methods for permafrost and ground ice studies, new and innovative ways of using these data must be explored. In addition to the primary data that these geophysical tools provide, it is possible that auxiliary information about the subsurface can be derived and linked with more broad-scale geomorphic investigations. For example, a major challenge in applying GPR to permafrost environments involves interpreting the depth of a reflector based on the signal's return time. When values of substrate permittivity are not known, the user must use estimated signal traveltime or bore or trench to a known reflector to calibrate

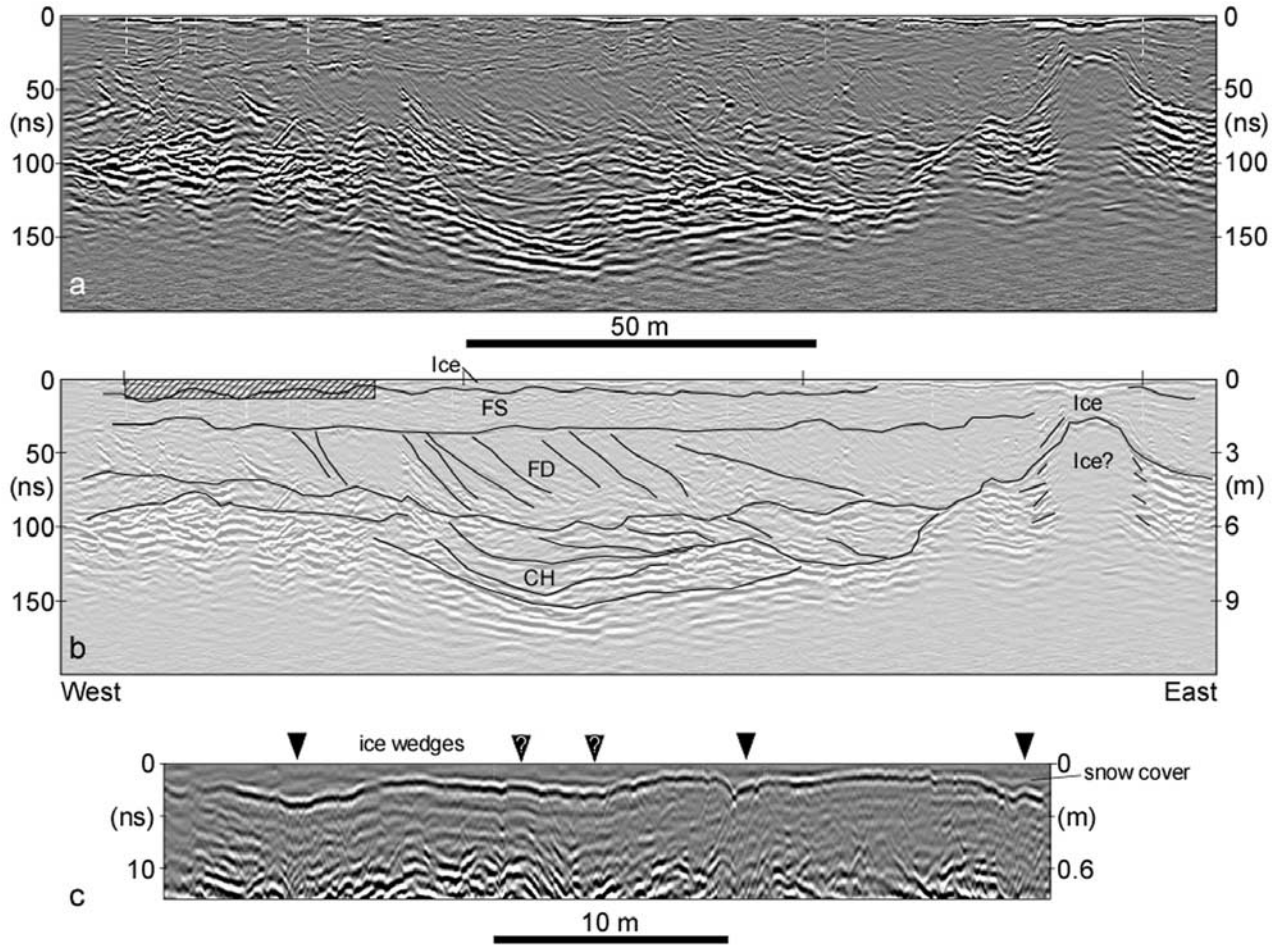

Figure 10. (a) GPR data from Site 303 collected at 200 MHz. (b) Interpretation showing the base of the active layer, frozen sediments (FS), foreset deposits (FD), a paleochannel (CH), and a massive ice body. Hatched box shows the area covered by the 900 MHz data. (c) The 900 MHz transect revealing the top ~75 cm of the snow cover and active layer. Triangles show locations of ice wedge troughs beneath the snow cover detected during the survey and slight near-vertical displacements in the data. Triangles with question marks are locations where the interpretation of wedge ice is less confident.

signal velocities. However, it is possible that these invasive and destructive methods could be replaced by the use of complementary tools such as CCR and GPR. Specifically, GPR and CCR utilize electromagnetic properties of the substrate, namely permittivity and resistivity. If resistivity values could be translated into permittivity, a precursory GPR/CCR survey at a given site would thereby eliminate the need to dig to a known reflector.

[37] Data collected at the outwash site demonstrate how both systems detect several of the same irregularly shaped bodies of massive ice surrounded by frozen sand. These interpretations were confirmed through direct observation and measurement of massive ice and frozen sand exposed in the adjacent sump wall. At Granular Resource Site 208, geophysical data indicated massive ground ice beneath the highest parts of a kame deposit but its absence beneath a vegetated depression. Because the depth of the depression is on the same order as the thickness of the massive ice layer beneath the adjacent ridges, we interpreted the structure as a thermokarst depression. This interpretation is also consistent with dipping stratigraphy observed in the GPR data. These results agree with observations by other researchers where massive ice was found beneath other ridges and positive relief features and the widespread indication of stabilized thermokarst [*Rampton and Mackay*, 1971; *Pollard and French*, 1980; *Rampton*, 1988; *Gowan and Dallimore*, 1992; *De Pascale*, 2005]. The relationship between massive ice and topography, and the degree to which this geophysical approach can assess massive ice occurrence, is an important aspect of ground ice mapping and landscape interpretation. In particular, the extent to which features like kames, eskers, pingos, and even moraines owe their relief to the presence of ground ice [*Rampton and Mackay*, 1971; *Rampton and Bouchard*, 1975; *Pollard and French*, 1980; *Harry et al.*, 1988] is an important consideration in permafrost terrain. Data collected at Granular Resource Site 303 indicated massive ice and ice-rich sediments to a depth of about 9 m underlain by ice-poor materials. The abrupt transition to ice-poor sediments and the irregular pattern of this contact, as well as stratigraphy revealed in the GPR data, could indicate an unconformity related to an older surface.

Table 2. Ranges in Resistivity Values for Several Materials Measured in March 2004

Material	Location	Resistivity Value Range (Ohm m)
Massive ice	Outwash site	10,000–25,000
Massive sand with 30% ice content	Outwash site	6,000–10,000
Frozen active layer	Outwash site	20,000–50,000
Massive Ice	Site 208	15,000–60,000
Ice wedges	Site 303	15,000–30,000

[38] This study demonstrates how geophysical surveys utilizing a combination of techniques, like CCR and GPR, not only have the potential to provide rapid and accurate information about permafrost and ground ice but reduce interpreter error and increase confidence in estimates of depth and material when both systems detect the same geologic structures. By comparison, boreholes or test pits, which in the past have been the main basis for the assessment of ground ice condition provide point information with little or no spatial confidence and also contribute to tundra disturbance. The spatially variable nature of permafrost limits the usefulness of point data, no matter how detailed. Borehole data are adequate for isopach mapping of ice occurrence; however, drilling costs for each borehole are high. It is therefore more cost-effective to assess permafrost conditions using CCR and GPR prior to any drilling program. The borehole results would then act to verify and calibrate the geophysical data, which is required for geophysical interpretation. By doing so, a better understanding of ground ice distribution can be obtained cheaply, without environmental disturbance, and at the same time provide information that can be used in the monitoring and prediction of thermokarst.

[39] Warming in the Arctic is occurring sooner and more rapidly that initially expected [*Arctic Climate Impact Assessment*, 2005] and will increase with time. Ground ice that has been preserved in the permafrost of the western Canadian Arctic since the late Pleistocene and early Holocene will experience higher temperatures and potentially increased melting. Although some of the ground ice detected in this study lies at depths greater than 5–10 m, all ground ice in the upper 10 m of permafrost is believed to be vulnerable to natural and human disturbances [*Pollard and French*, 1980]. A monitoring program that targets ice-rich landscapes should be developed to understand and predict future geomorphologic changes to the landscape. With the ability to detect changes in known ground ice bodies and the potential to detect the ground ice in formerly unexplored sediments, areas sensitive to change (thermokarst) can be identified and adaptation and remediation plans can be developed for communities and infrastructures in permafrost.

8. Conclusions

[40] Fieldwork on ground ice characterization of granular deposits on Richards Island in the Mackenzie Delta utilizing noninvasive geophysical methods like CCR and GPR provided an opportunity to assess the synergistic benefits of using two complementary geophysical systems. Our results support previous research showing that, individually, CCR and GPR are useful tools for obtaining general subsurface information in permafrost [e.g., *Calvert*, 2002; *Dallimore and Davis*, 1987; *Arcone et al.*, 1998; *Moorman et al.*, 2003] and clearly show the added value that results by combining their outputs. Combined data from both systems collected along the same transects at the same time results in more stratigraphic detail and higher confidence interpretations than can be achieved by either of the instruments alone.

[41] This study also provides the first description of a comprehensive workflow of CCR data, from acquisition through data processing and interpretation in a permafrost environment. By investigating a number of sites in a short period of time during March 2004, characteristic resistivity values for different permafrost materials were obtained (Table 2). Cold ground temperatures coupled with winter fieldwork simplifies both the field program (i.e., surveys are easier from a stable hard snow platform) and the data interpretation. Cold ground temperatures ($\sim -14^{\circ}$C at the ground surface and -10°C at depth) eliminate liquid water and brine films from the permafrost system, especially the active layer, and thus reduce signal loss and data complexity and improve interpretation. The conductive nature of liquid water and brine films that are more common at warmer permafrost temperatures can mask the high ice contents of some ice-rich deposits. CCR surveys have an advantage over other resistivity methods in permafrost environments because data are collected as the instrument is pulled across the ground. This allows a faster survey and the ability to collect data easily in winter and spring when galvanic coupling methods are difficult due to snow cover. In this study, two commercially available geophysical tools were used in very cold conditions (-40°C) with few operational problems.

[42] This is also the first permafrost research utilizing both CCR and GPR tools as part of the same cryostratigraphic assessment and ground ice interpretation (namely wedge and massive ice). One of the most useful outcomes of this research is the conclusion that the analysis of dielectric and resistivity transitions (reflectors) clearly indicates stratigraphic contacts between massive ice and other materials when using both systems. This has valuable implications for mapping the extent of massive ice bodies, depth to massive ice, and their lower contacts. By its nature, pore ice is more difficult to detect because it fills the pore space of sediments, altering the material properties without producing a discrete target in the geophysical data.

[43] In conclusion this study provides strong support for the use of complementary geophysical tools to map ground ice. CCR and GPR techniques, when used in concert yield subsurface information regarding both materials and geometries that cannot be well constrained using either one of the techniques alone. We were able to resolve wedge ice, massive ice, zones of thermokarst, and ice-rich sediments in our investigations; however, our data confirm that individual ice lenses are generally too small to be identified uniquely and the GPR signal tends to show increasing scatter with increasing ice lens volumes. However, permittivity values of the scattered signals could be used to calculate relative ice volumes within the permafrost. For ground ice bodies larger than the theoretical resolution of the GPR signal (1/4 wavelength), the difference in permittivity values between ice and the enclosing sediments generates a strong, distinguishable reflector. Massive ice

lends itself especially well to detection by GPR. Because near-pure ice has virtually a very low dielectric constant ($\varepsilon \sim 3$), it readily transmits the GPR signal. Therefore, both the top and bottom of a massive ice deposit should be detectable because of the strong reflector at the ice-sediment interfaces. In the case of CCR, a drastic increase in resistivity occurs at the freezing point and thus the resistivity of frozen soils is generally 10–1000 times greater than that of unfrozen soils. Similar to GPR, signal attenuation lessens with decreasing liquid water content; consequently, CCR is extremely useful for permafrost applications because the frozen ground allows for enhanced signal propagation, permitting delineation of different materials. Ultimately, GPR can help define stratigraphic context, while CCR can delineate cryostratigraphy for a given study site. When used together, they can assist in developing subsurface maps of ground ice distribution. Further testing of different materials is needed before direct correlation can be made between raw permittivity and resistivity data.

[44] **Acknowledgments.** The authors thank T. Jorgenson, an anonymous reviewer, and the editors of JGR–Earth Surface for comments that improved the manuscript. Funding for this research was provided by a NSERC Discovery grant, ArcticNet, and a PERD/DIAND financial agreement managed by R. Gowan with McGill University (W. Pollard). Support for K. Williams was from a Smithsonian Institution Becker Endowment Grant. Field support for this research was provided by the Aurora Research Institute (ARI) in Inuvik and was conducted under NWT research licenses 13560 and 13753 and Inuvialuit Land Administration (ILA) license 03TIN055. Les Kutny assisted with field equipment and logistics in Inuvik.

References

Arcone, S. A., D. E. Lawson, and A. J. Delaney (1995), Short-pulse radar wavelet recovery and resolution of dielectric contrast within englacial and basal ice of Matanuska Glacier, Alaska, USA, *J. Glaciol.*, *41*, 68–86.

Arcone, S. A., D. E. Lawson, A. J. Delaney, J. C. Strasser, and J. D. Strasser (1998), Ground penetrating radar reflection profiling of groundwater and bedrock in an area of discontinuous permafrost, *Geophysics*, *63*, 1573–1584.

Arctic Climate Impact Assessment (2005), *Arctic Climate Impact Assessment*, 1042 pp., Cambridge Univ. Press, Cambridge, U. K.

Baines, D., D. G. Smith, D. G. Froese, P. Bauman, and G. Nimeck (2002), Electrical resistivity ground imaging (ERGI): A new tool for mapping the lithology and geometry of channel-belts and valley-fills, *Sedimentology*, *49*, 441–449.

Calvert, H. T. (2002), Capactive-coupled resistivity survey of ice-bearing sediments, Mackenzie Delta, Canada, paper presented at 72nd Annual Meeting, Soc. of Explor, Geophys., Salt Lake City, Utah.

Calvert, H. T., S. R. Dallimore, and J. A. Hunter (2001), Application of geophysical techniques for mapping of ice-bearing sediments, Mackenzie Delta, western Arctic, Canada, paper presented at Conference on the Geophysical Detection of Subsurface Water on Mars, Lunar and Planet. Inst., Houston, Tex.

Dallimore, S. R., and J. L. Davis (1987), Ground probing radar investigations of massive ground ice and near surface geology in continuous permafrost, in *Current Research Part A*, *Pap. Geol. Surv. Can.*, *87-01A*, 913–918.

Dallimore, S. R., J. L. Davis, and J. A. Pilon (1992), Ground penetrating radar investigations of massive ground ice, in *Ground Penetrating Radar*, *Pap. Geol. Surv. Can.*, *90-04*, 41–48.

Davis, J. L., and A. P. Annan (1989), Ground-penetrating radar for high-resolution mapping of soil and rock stratigraphy, *Geophys. Prospect.*, *37*, 531–551.

De Pascale, G. P. (2005), Occurrence of massive ice in coarse-grained deposits, western Canadian Arctic, M.Sci. thesis, 122 pp., McGill Univ., Montreal, Canada, 2 June.

Doolittle, J. A., M. A. Hardisky, and M. F. Gross (1990), A ground penetrating radar study of active layer thicknesses in areas of moist sedge and wet sedge tundra near Bethel, Alaska, U.S.A., *Arct. Alpine Res.*, *22*, 175–182.

EBA Engineering Consultants Ltd. (EBA) (1987), Compilation of borehole logs for the Mackenzie Delta area, N. W. T., vols. 1 and 2, Ottawa, Ont., Canada.

Fountain, A. G., and R. W. Jacobel (1997), Advances in ice studies of a temperate alpine glacier, South Cascade Glacier, Washington, USA, *Ann. Glaciol.*, *24*, 303–308.

Geometrics, Inc. (2001) Data Map OhmMapper User Guide 29006-01, Rev 3.0, Manual 2900701, 55 pp., San Jose, Calif.

Gowan, R. J., and S. R. Dallimore (1992), Ground ice associated with granular deposits in the Tuktoyaktuk coastlands area, N. W. T., in *Proceedings of the Fifth Canadian Permafrost Conference*, *Collect. Nord.*, *54*, 283–290.

Harry, D. G., H. M. French, and W. H. Pollard (1988), Massive ground ice and ice-cored terrain near Sabine Point, Yukon Coastal Plain, *Can. J. Earth Sci.*, *25*, 1846–1856.

Hauck, C. (2002), Frozen ground monitoring using DC resistivity tomography, *Geophys. Res. Lett.*, *29*(21), 2016, doi:10.1029/2002GL014995.

Hauck, C., and C. Kneilsel (2006), Application of capacitively-coupled and DC electrical resistivity imaging for mountain permafrost studies, *Permafrost Periglacial*, *17*, 169–177.

Hauck, C., D. V. Muhll, and H. Maurer (2003), Using DC resistivity tomography to detect and characterize mountain permafrost, *Geophys. Prospect.*, *51*, 273–284.

Hinkel, K. M., J. A. Doolittle, J. G. Bockheim, F. E. Nelson, R. Paetzold, J. M. Kimble, and R. Travis (2001), Detection of subsurface permafrost features with ground penetrating radar, Barrow, Alaska, *Permafrost Periglacial. Process*, *12*, 179–190.

Hoekstra, P., P. V. Sellman, and A. Delaney (1975), Ground and airborne resistivity surveys of permafrost near Fairbanks, Alaska, *Geophysics*, *40*, 641–656.

Ishikawa, M., W. Teiji, and N. Naohiro (2001), Genetic differences of rock glaciers and the discontinuous mountain permafrost zone in Kanchanjunga Himal, eastern Nepal, *Permafrost Periglacial Process*, *12*, 243–253.

Kneisel, C., C. Hauck, and D. Vonder Mühll (2000), Permafrost below the timberline confirmed and characterized by geoelectrical resistivity measurements, Bever Valley, Eastern Swiss Alps, *Permafrost Periglacial Process*, *11*, 295–304.

Loke, M. H. (1999), RES2DINV ver. 3.42, Geolectrical Imaging 2D & 3D, User Manual, Terraplus Inc., Richmond Hill, Ont., Canada.

Loke, M. H., and R. Barker (1996), Rapid least-squares inversion of apparent resistivity pseudo-sections using a quasi-Newton method, *Geophys. Prospect.*, *44*, 131–152.

Mackay, J. R. (1963), The Mackenzie Delta Area, NET, Ottawa, *Memoir 8*, 202 pp., Geogr. Branch, Mines and Tech. Surv., Ottawa, Ont., Canada.

Mackay, J. R. (1972), The world of undeground ice, *Ann. Assoc. Am. Geogr.*, *62*, 1–22.

Mackay, J. R. (1979), Pingos of the Tuktoyaktuk Peninsula area, Northwest Territories, *Geogr. Phys. Quat.*, *33*, 3–61.

Mackay, J. R. (1998), Pingo growth and collapse, Tuktoyaktuk Peninsula Area, western Arctic Coast, Canada: A long-term field study, *Geogr. Phys. Quat.*, *52*, 271–323.

Mackay, J. R. (1999), Periglacial features developed on the exposed lake bottoms of seven lakes that drained rapidly after 1950, Tuktoyaktuk Peninsula area, western Arctic coast, Canada, *Permafrost Periglacial Processes*, *10*(1), 39–63.

Mackay, J. R., and S. R. Dallimore (1992), Massive ice of the Tuktoyaktuk area, western Arctic coast, Canada, *Can. J. Earth Sci.*, *29*, 1235–1249.

Marescot, L., M. H. Loke, D. Chapellier, R. Delaloye, C. Lambiel, and E. Reynard (2003), Assessing reliability of 2D resistivity imaging in mountain permafrost studies using the depth of investigation index method, *Near Surface Geophys.*, *1*, 57–67.

Moorman, B. J. (1994), Ground penetrating radar investigations of woodchip-covered slopes along the Norman Wells pipeline in the Northwest Territories, *Geol. Surv. Can. Open File*, *2889*, 125 pp.

Moorman, B. J. (1995), Geotechnical investigations of woodchip slopes along the Norman Wells Pipeline (Northwest Territories): Analysis of 1993 ground penetrating radar data, *Geol. Surv. Can. Open File*, *3024*, 230 pp.

Moorman, B. J., and F. A. Michel (2000), The burial of ice in the proglacial environment on Bylot Island, Arctic Canada, *Permafrost Periglacial Process*, *11*, 161–175.

Moorman, B. J., S. D. Robinson, and M. M. Burgess (2003), Imaging periglacial conditions with ground-penetrating radar, *Permafrost Periglacial Process*, *14*, 319–329.

Murray, T., T. L. Dion, and G. W. Stuart (1997), Locating englacial water using GPR, Falljökull, Iceland, *Ice*, *113/114*, 29.

Murton, J. B., and H. M. French (1994), Cryostructures in permafrost, Tuktoyaktuk Coastlands, western Arctic Canada, *Can. J. Earth Sci.*, *31*, 737–747.

Murton, J. B., R. Waller, J. K. Hart, C. Whiteman, W. H. Pollard, and I. Clark (2004), Stratigraphy and glaciotectonic structures of permafrost deformed beneath the northwest margin of the Laurentide Ice Sheet, Tuktoyaktuk Coastlands, Canada, *J. Glaciol.*, *50*(170), 399–411.

Murton, J. B., C. A. Whiteman, R. I. Waller, W. H. Pollard, S. R. Dallimore, and I. Clark (2005), Basal ice facies and supraglacial melt-out till of the Laurentide Ice Sheet, Tuktoyaktuk Coastlands, western Arctic Canada, *Quat. Sci. Rev.*, *24*, 681–705.

Permafrost Subcommittee (1988), Glossary of permafrost and related ground-ice terms, *Tech. Mem. 142*, 156 pp., Assoc. Comm. on Geotech. Res., Natl. Res. Counc. of Can., Ottawa, Ont., Canada.

Pollard, W. H. (2005), Thermokarst, in *Encyclopedia of the Arctic*, edited by M. Nuttall, Fitsroy Dearborn, London.

Pollard, W. H., and H. M. French (1980), A first approximation of the volume of ground ice, Richard Island, Pleistocene Mackenzie delta, NWT, *Can. Geotech. J.*, *17*, 509–516.

Rampton, V. N. (1972), An outline of the Quaternary geology of the lower Mackenzie Region, in Mackenzie Delta Area Monograph, edited by D. Kerfoot, pp. 7–14, Brock Univ., St. Catharines, Ont., Canada.

Rampton, V. N. (1979), Surficial geology of Richards Island, District of Mackenzie, *Map 32-1979*, Geol. Surv. of Can., Ottawa, Ont.

Rampton, V. N. (1988), Quaternary Geology of the Tuktoyaktuk coastlands, Northwest Territories. *Mem. 423*, 98 pp., Geol. Surv. of Can., Ottawa, Ont.

Rampton, V. N., and M. Bouchard (1975), Surficial geology of Tuktoyaktuk, District of Mackenzie, *Geol. Surv. Can. Pap.*, 74-53.

Rampton, V. N., and J. R. Mackay (1971), Massive ice and icy sediments throughout the Tuktoyaktuk Peninsula, Richards Island, and nearby areas District of Mackenzie, *Geol. Surv. Can. Pap.*, 71-21.

Robinson, S. D. (1994), Geophysical studies of massive ground ice, Fosheim Peninsula, Ellesmere Island, Northwest Territories; *Current Research 1994–B*, pp. 11–18, Geol. Surv. of Can., Ottawa, Ont.

Robinson, S. D., B. J. Moorman, A. S. Judge, and S. R. Dallimore (1993), The characterization of massive ground ice At Ya-Ya Lake, Northwest Territories using radar stratigraphy techniques, in *Current Research, Part B, Interior Plains and Arctic Canada*, *Geol. Surv. Can. Pap.*, *93-01B*, 23–32.

Timofeev, V. M., A. W. Rodozinski, J. A. Hunter, and M. Douma (1994), A new ground resistivity method for engineering and environmental geophysics, paper presented at the Symposium on the Application of Geophysics to Engineering and Environmental Problems, Environ. and Eng. Geophys. Soc., Keystone, Colo.

Wolfe, S. A., M. M. Burgess, M. Douma, C. Hyde, and S. Robinson (1996), Geological and Geophysical Investigations of the Canamera Carat Lake Esker–Delta Complex, Slave Geological Province, NWT, 38 pp., Geol. Surv. of Can., Ottawa, Ont.

Wolfe, S. A., M. M. Burgess, M. Douma, C. Hyde, and S. Robinson (1997), Geological and geophysical investigations of massive ground ice in glaciofluvial deposits, Slave geological province, Northwest Territories, *Geol. Surv. Can. Open File*, *3442*, 107 pp.

G. P. De Pascale, William Lettis and Associates, Inc., Earth Science Consultants, 1777 Botelho Drive, Suite 262, Walnut Creek, CA 94596, USA.

W. H. Pollard, Department of Geography, McGill University, Burnside Hall Room 705, 805 Sherbrooke Street West, Montreal, QC, Canada H3A 2K6. (wayne.pollard@mcgill.ca)

K. K. Williams, Department of Earth Sciences and Science Education, Buffalo State College, 1300 Elmwood Avenue, Buffalo, NY 14222, USA.